Magnetotransport in a pseudomorphic $GaAs/Ga_{0.8}In_{0.2}As/Ga_{0.75}Al_{0.25}As$ heterostructure with a Si δ-doping layer

M. van der Burgt*
Department of Physics, Clarendon Laboratory, University of Oxford, Parks Road, Oxford OX1 3PU, United Kingdom

V. C. Karavolas and F. M. Peeters
Department of Physics, University of Antwerp (UIA), B-2610 Antwerpen, Belgium

J. Singleton and R. J. Nicholas
Department of Physics, Clarendon Laboratory, University of Oxford, Parks Road, Oxford OX1 3PU, United Kingdom

F. Herlach
Department of Physics, Katholieke Universiteit Leuven, Celestijnenlaan 200D, B-3001 Leuven, Belgium

J. J. Harris
Interdisciplinary Research Centre for Semiconductor Materials, Imperial College, Prince Consort Road, London SW7 2BZ, United Kingdom

M. Van Hove and G. Borghs
Interuniversity Microelectronics Center, Kapeldreef 75, B-3001 Leuven, Belgium
(Received 24 May 1995)

Magnetotransport properties of a pseudomorphic $GaAs/Ga_{0.8}In_{0.2}As/Ga_{0.75}Al_{0.25}As$ heterostructure are investigated in pulsed magnetic fields up to 50 T and at temperatures of T =1.4 and 4.2 K. The structure studied consists of a Si δ layer parallel to a $Ga_{0.8}In_{0.2}As$ quantum well (QW). The dark electron density of the structure is $n_e = 1.67 \times 10^{16}$ m^{-2}. By illumination the density can be increased up to a factor of 4; this way the second subband in the $Ga_{0.8}In_{0.2}As$ QW can become populated as well as the Si δ layer. The presence of electrons in the δ layer results in drastic changes in the transport data, especially at magnetic fields beyond 30 T. The phenomena observed are interpreted as (i) magnetic freeze-out of carriers in the δ layer when a low density of electrons is present in the δ layer, and (ii) quantization of the electron motion in the two-dimensional electron gases in both the $Ga_{0.8}In_{0.2}As$ QW and the Si δ layer in the case of high densities. These conclusions are corroborated by the numerical results of our theoretical model. We obtain satisfactory agreement between model and experiment.

I. INTRODUCTION

Since the discovery of the two-dimensional electron gas (2DEG) at the interface of a $GaAs/Ga_{1-x}Al_xAs$ heterojunction,[1] the physical properties of 2DEG's in III-V semiconductors have been intensively investigated. One of the basic requirements for fast electronic devices based on such semiconductor 2DEG's is a high conductivity. In modulation-doped $GaAs/Ga_{1-x}Al_xAs$ heterostructures[2] grown by molecular-beam epitaxy, electron mobilities as high as 1000 m^2/V s can be achieved at temperatures below 4 K.[3] However, the two-dimensional (2D) electron densities in these high-mobility systems are usually not much larger than a few times 10^{15} m^{-2}.[3,4] At high temperatures the mobility in 2D GaAs based systems is strongly limited by optical phonon scattering.[5–8] Therefore, high electron densities are needed in order to achieve high room-temperature conductivities. Much greater densities of 2D electrons then in $GaAs/Ga_{1-x}Al_xAs$ structures can be accommodated in $GaAs/Ga_{1-x}In_xAs/Ga_{1-y}Al_yAs$ systems.[9] This is due to the large conduction-band offset,[10–12] which results in larger confinement energies for the 2D electrons. When the $Ga_{1-x}In_xAs$ layer is thin enough the lattice mismatch between $Ga_{1-x}In_xAs$ and $Ga_{1-y}Al_yAs$ is accommodated by the $Ga_{1-x}In_xAs$ layer without introducing misfit dislocations,[13,14] resulting in a pseudomorphic structure.

The electron concentrations in $GaAs/Ga_{1-x}In_xAs/Ga_{1-y}Al_yAs$ structures can be further increased by making use of a δ-function-like doping profile[15,16] instead of a uniformly Si-doped $Ga_{1-y}Al_yAs$ layer. This also results in an enhanced mobility[17,18] as compared to modulation-doped structures with uniformly doped layers. In this way, electron densities higher than 1.5×10^{16} m^{-2} and low-temperature mobilities of $\mu \approx 3$–4 m^2/V s can be achieved. The high densities and mo-

bilities and the resulting high-room temperature conductivities in these systems make them attractive for use in high-performance high-electron-mobility transistors (HEMT's).[19]

The presence of deep impurity levels known as DX centers in Si-doped $Ga_{1-x}Al_xAs$ with $x \geq 0.20$ is responsible for the persistent photoconductivity in this material.[20–22] The ionization of the DX centers after illumination can lead to a parallel conducting channel in modulation-doped heterostructures as carriers do not recombine with the ionized DX centers.[23] Since the carriers in the parallel layer have a low mobility compared to the 2D electrons in the quantum well (QW) or at the heterojunction interface, parallel conduction is usually regarded as an undesirable effect that degrades the performance of a HEMT.[24,25] Most studies of parallel conduction are therefore mainly concerned with the question of how to avoid it[26] or how to extract mobilities and densities of the different conducting channels.[27,28] In this paper we will show that conduction in a δ layer parallel to a $Ga_{0.8}In_{0.2}As$ QW can give rise to interesting effects in high magnetic fields, which are due to the interplay between the 2D carriers in the δ layer and the $Ga_{0.8}In_{0.2}As$ QW, and the 2D character of the carriers in the Si δ layer in the $Ga_{1-x}Al_xAs$. The 2D character of electrons in a Si δ layer in GaAs was demonstrated by Zrenner *et al.*[15] In high magnetic fields a metal-insulator transition due to magnetic freeze-out was observed in δ-doped GaAs systems.[29,30]

We report transport measurements in pulsed magnetic fields up to 50 T on a $GaAs/Ga_{0.8}In_{0.2}As/Ga_{0.75}Al_{0.25}As$ structure with a Si-doped δ layer in the $Ga_{0.75}Al_{0.25}As$ layer. The initial data, together with a brief qualitative description, were presented in two previous works.[31,32] In this paper we want to give a description of the data together with a full theoretical modeling over the whole experimental field range.

In the system studied, the density of conduction electrons can be increased by illuminating the sample with red light. At the lowest electron densities the quantized Hall effect (QHE) is observed, with one subband occupied in the $Ga_{0.8}In_{0.2}As$ QW. As the density is increased the second subband becomes populated. Further increases of the electron density result in parallel conduction in the δ layer, which leads to drastic changes in the transport coefficients ρ_{xx} and ρ_{xy}, especially at fields above 30 T. These are attributed to magnetic freeze-out in the δ layer. With the δ layer parallel to a conducting 2DEG in the $Ga_{0.8}In_{0.2}As$ QW, it is possible to study magnetic freeze-out without the problems of a diverging resistance in the δ layer. At the highest electron concentrations the QHE is observed in both the $Ga_{0.8}In_{0.2}As$ QW and the Si δ layer.

The experimental arrangements are described in Sec. II. In Sec. III a brief discussion of the transport data is presented using solutions of the coupled Poisson and Schrödinger equations, which gives a qualitative picture of the different subbands in the $Ga_{0.8}In_{0.2}As$ QW and in the Si δ layer. The results of the two-carrier analysis of the low-field transport data (Sec. IV) are used to model the conductivity tensor for high magnetic fields (Sec. V). The theoretical description of the high-field data combines some existing theoretical models, resulting in an accurate description of the measured ρ_{xx} and ρ_{xy} data for the whole field range up to 50 T.

II. EXPERIMENTAL DETAILS

The transport experiments described in this paper were performed on a modulation-doped pseudomorphic GaAs/ $Ga_{0.8}In_{0.2}As/Ga_{0.75}Al_{0.25}As$ heterostructure grown by molecular-beam epitaxy. The structure of the sample is shown in Fig. 1. It consists of a 13-nm-thick $Ga_{0.8}In_{0.2}As$ layer[33] grown on a GaAs substrate with a GaAs buffer, followed by a 5-nm-wide $Ga_{0.75}Al_{0.25}As$ spacer layer, a Si δ-layer with a Si concentration of 5×10^{16} m^{-2}, a 30-nm-thick Si-doped (5×10^{23} m^{-3}) $Ga_{0.75}Al_{0.25}As$ layer, and an n^+-GaAs cap layer of approximately 5 nm. The samples were mesa etched into 55-μm-wide Hall bars. Two samples from two wafers with a nominally identical structure were studied (only the thickness of the n^+-GaAs cap layer was slightly different); the results from the two samples were almost identical and so only the results of one will be discussed in this paper.

Through the persistent photoconductivity effect in the $Ga_{0.75}Al_{0.25}As$ layer, the electron density in the sample studied can be increased by illumination with a red light-emitting diode. The electron density is $n_e = 1.67 \times 10^{16}$ m^{-2} and the mobility is $\mu = 3.2$ m^2/V s when the sample is cooled to 4.2 K in the dark. After sufficient illumination the total electron density can be increased by a factor of almost 4. The structure of the conduction band of the sample under different illumination conditions is shown in Fig. 2 and is further discussed in Sec. III.

The experiments were done in a liquid helium bath cryostat at temperatures of T=1.4 and 4.2 K in two different pulsed magnetic field facilities.[34,35] In both installations the magnetic field is generated by discharging a capacitor bank into a reinforced solenoid immersed in liq-

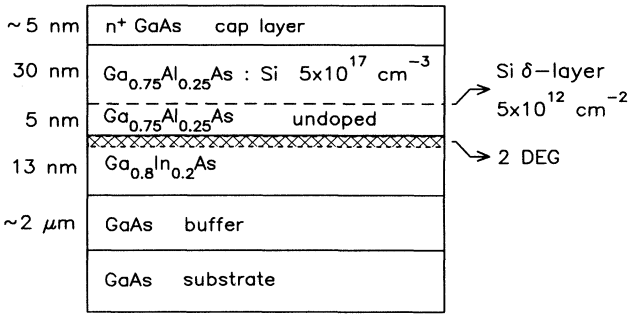

FIG. 1. Structure of the studied pseudomorphic $GaAs/Ga_{0.8}In_{0.2}As/Ga_{0.75}Al_{0.25}As$ system. At 5 nm from the $Ga_{0.8}In_{0.2}As$ QW a Si δ layer is grown.

uid nitrogen; maximum fields between 45 and 50 T can be achieved in both systems. The pulse shape is half a period of a damped sine wave, which reaches its peak after 4–8 ms; the total pulse duration can be varied in the range 15–40 ms.

Both the Hall effect ρ_{xy} and the longitudinal magnetoresistance ρ_{xx} were measured using dc currents in the range 1–10 μA. Due to its high carrier density, the high-field magnetoresistance of the sample is relatively low (≈ 30 kΩ in fields up to 50 T) compared to high-mobility GaAs/$Ga_{1-x}Al_xAs$ heterojunctions, which have mostly a low carrier density. Therefore the distortions seen in transport measurements on a 2DEG in transient magnetic fields described in Ref. 36 are negligible for the data taken during the down sweep of the pulse. The down sweep is generally a few milliseconds longer than the up sweep, so that the signal to noise ratio of the data taken during the down sweep is usually slightly better. Although there is usually good agreement between the data from the up and the down sweep, for clarity only data taken during the down sweep are shown in the following sections. The voltages measured on the sample are amplified by a PARC/EG&G differential amplifier Model 113 or 5113 and recorded by a fast digital transient recorder. The data are then transferred to a personal computer. The magnetic field is determined by measuring the induced voltage in a pickup coil with an accurately known area, mounted in the vicinity of the sample. More details about transport measurements in pulsed magnetic fields can be found in Ref. 37.

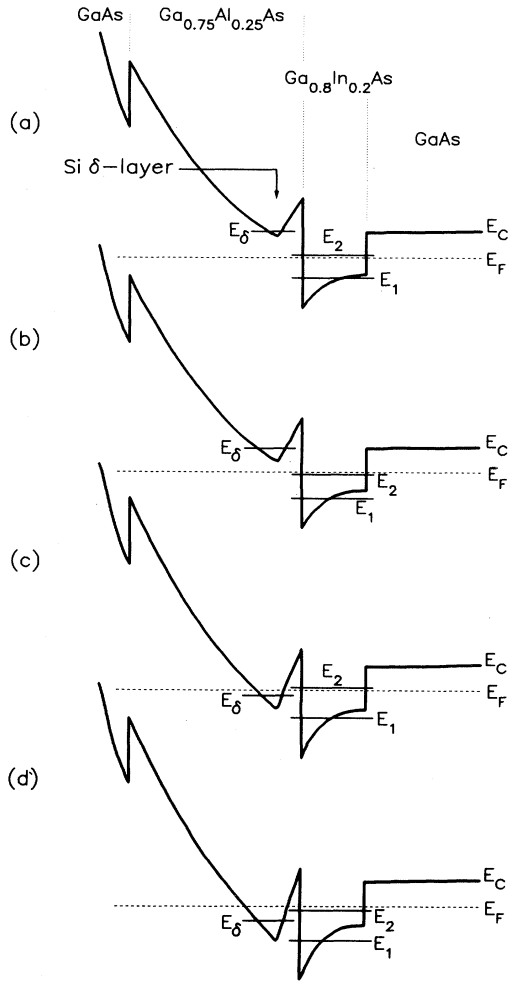

FIG. 2. Structure of the conduction band (E_C) under different illumination conditions. In the unilluminated sample (a), just one subband E_1 in the $Ga_{0.8}In_{0.2}As$ well is occupied. When the structure is illuminated, the second subband E_2 in the $Ga_{0.8}In_{0.2}As$ well becomes populated (b). Further illumination brings the lowest level E_δ in the δ layer below the Fermi level E_F and E_2 depopulates (c). When the density is satured, both subbands in the $Ga_{0.8}In_{0.2}As$ QW and E_δ in the δ layer are occupied (d).

III. BAND STRUCTURE

In order to get a qualitative picture of how the different subbands in the $Ga_{0.8}In_{0.2}As$ and in the δ layer behave when the carrier density is increased by illumination, we calculated the subband structure by solving the coupled Poisson-Schrödinger equations self- consistently.[38,39] The persistent photoconductivity effect can be mimicked in these calculations by reducing the ionization energy of the Si donors. A smaller ionization energy results in a higher density of ionized donors and consequently a higher electron density in the conduction band. Since the shape and the population of the conduction band influences the magnetic-field dependence of the transport coefficients ρ_{xx} and ρ_{xy}, this section also summarizes our basic conclusions about the transport data.

An overview of the changes in the conduction band with illumination is shown in Fig. 2. Figure 2(a) shows the band structure in the unilluminated sample: only the lowest subband E_1 is occupied. Under these circumstances we observe the quantized Hall effect due to the 2DEG in this subband.

A small dose of illumination results in the occupation of the second subband E_2 of the $Ga_{0.8}In_{0.2}As$ quantum well [Fig. 2(b)]. As we will see in Sec. IV, this clearly shows up in the low-field ρ_{xx} data as a beat of two frequencies in the Shubnikov–de Haas (SdH) oscillations. As the Fermi level E_F still lies below the lowest states in the δ layer, no carriers are found in this layer.

A further increase in carrier density results in the occupation of the Si impurity layer when the lowest state in the δ layer E_δ falls below the Fermi energy [Fig. 2(c)]; at this point no obvious sign of the second subband E_2 in the $Ga_{0.8}In_{0.2}As$ remains in the transport data. The reason for this is that E_δ falls below E_2 and so this subband is consequently depopulated. As will be shown in Sec. V, at low densities in the δ layer ($< 1 \times 10^{16}$ m^{-2}) and sufficiently high magnetic fields (> 20 T), a metal-insulator transition occurs in the δ layer.

The band structure at saturated or nearly saturated densities is illustrated in Fig. 2(d). Two subbands are again occupied in the $Ga_{0.8}In_{0.2}As$ quantum well. Due

to the small number of carriers in the second subband as compared to these in the first subband and in the δ layer, the contribution of the second subband to the conductivity is small and in fact does not show up in the transport data. The electron density in the δ layer is then sufficiently large such that we can treat these electrons as a second 2DEG. The transport data then show a superposition of the QHE from both the $Ga_{0.8}In_{0.2}As$ quantum well and the Si δ layer.

IV. SMALL MAGNETIC FIELDS

A. Theory

In the low-magnetic-field range the SdH oscillations in the resistivity ρ_{xx} of a single subband can be described by the model of Isihara and Smrčka,[40] which was improved by Coleridge *et al.*[41] by the introduction of two distinct relaxation times. Since at low fields the cyclotron orbit of an electron has a large spatial extent this model takes into account multiple scattering. The calculation of the conductivity is based on a constant density of states (DOS) $g_0 = m^*/\pi\hbar^2$ (m^* is the effective mass and $\hbar$ is Planck's constant over 2π) with a sinusoidal oscillating part superimposed. The oscillating part of the DOS reflects the onset of Landau quantization and leads to the SdH oscillations in the magnetoconductivity.

The conductivity tensor given by Coleridge *et al.*[41] can be inverted to give the resistivities ρ_{xx} and ρ_{xy}. For small magnetic fields the resistivity ρ_{xx} can be written as[38,41]

$$\rho_{xx} = \rho_0 \left[1 - 4e^{-\pi/\omega_c\tau_q} \frac{X}{\sinh X} \cos\left(\frac{2\pi E_F}{\hbar\omega_c}\right)\right]. \quad (1)$$

In this expression ρ_0 is the zero-field resistivity, $\omega_c = eB/m^*$ is the cyclotron frequency, $E_F = \pi\hbar^2 n_e/m^*$ is the Fermi energy, $X = 2\pi^2 k_B T/\hbar\omega_c$, and k_B is Boltzmann's constant. Both the *transport* scattering time $\tau_t = m^*/\rho_0 e^2 n_e$ and the *single-particle* scattering time τ_q are present in this expression. In modulation-doped 2D systems these can differ by more than an order of magnitude.[42–45] The zero-field resistivity ρ_0 is determined by the classical or transport scattering time τ_t, while the single-particle relaxation time or quantum-mechanical scattering time τ_q is present in the oscillatory part of the DOS. The transport scattering rate $1/\tau_t$ contains no contribution from forward scattering and small-angle scattering receives a very small weight, as these scattering events have a very limited effect on the electron drift velocity. In the single-particle scattering rate $1/\tau_q$, however, every scattering event is equally important.

The single-particle scattering time τ_q can be determined from the decay of the amplitude of the SdH oscillations with decreasing magnetic field. The temperature dependence of the oscillations is given by the factor $X/\sinh X$ in Eq. (1). Since ω_c contains the effective mass m^*, measuring the amplitude of the oscillations as a function of temperature allows the determination of m^*. The cosine factor in Eq. (1) shows that the SdH oscillations are periodic in inverse magnetic field. The carrier density of the 2D subband is determined by measuring the period.

This model is valid for low and intermediate fields such that $\omega_c\tau_q \leq 1$. For larger magnetic fields localization of the electrons away from the center of the Landau level[46,47] starts to play an important role, so that the above model is no longer valid.[41,48]

B. Experimental results

Densities, transport mobilities, and transport scattering times can be obtained from the low-field $B \to 0$ limit of the transport coefficients ρ_{xx} and ρ_{xy}. We measured the Hall density n_H from the slope of the Hall resistance at low magnetic fields

$$\rho_{xy}(B \to 0) = B/n_H e. \quad (2)$$

The Hall mobility μ_H is then defined by

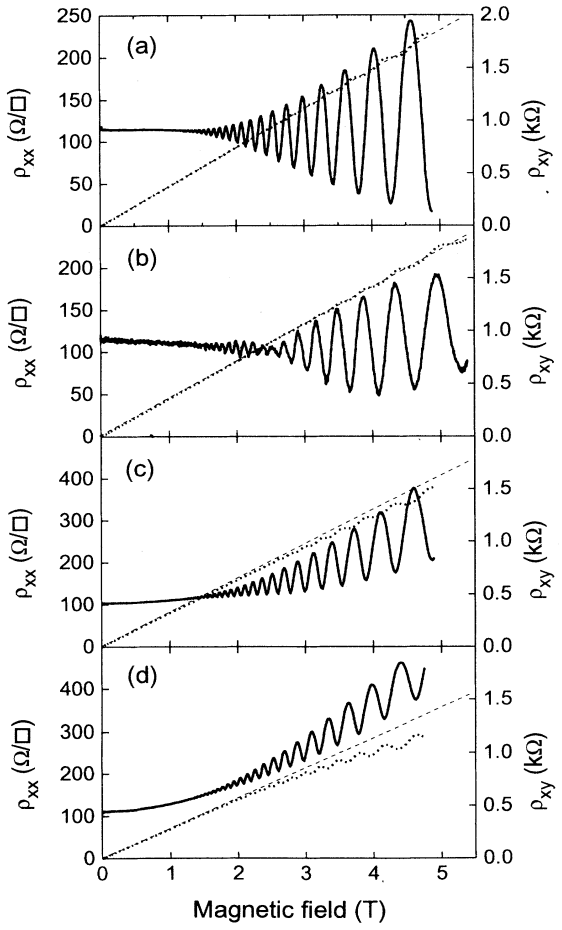

FIG. 3. Low-field data for ρ_{xx} (full line) and ρ_{xy} (dotted line) for four different Hall densities: $n_H = 1.67$ (a), 1.75 (b), 1.97 (c), and 2.21×10^{16} m^{-2} (d). The dashed line represents the classical Hall resistance for a single carrier system with density n_H.

$$\rho_{xx}(B=0)=\rho_0=1/n_H\mu_H e. \quad (3)$$

For a single-carrier system the Hall density is equal to the total density and the Hall mobility is given by $\mu_H = e\tau_t/m^*$. When more then one type of carrier is present μ_H represents a weighed average mobility (see Sec. IV C).

The 4.2 K resistivities ρ_{xx} and ρ_{xy} in fields up to 5 T are shown in Fig. 3 for four different densities. After cooling in the dark, $n_H = 1.67 \times 10^{16}$ m^{-2} and ρ_{xx} shows a single series of SdH oscillations on a constant background [Fig. 3(a)]. The Hall effect ρ_{xy} is a straight line on which plateaus start to develop above 2.5 T. This behavior of ρ_{xx} and ρ_{xy} indicates that there is only one type of carrier involved in the conduction process at this density.[41,44,49]

At a Hall density of $n_H = 1.75 \times 10^{16}$ m^{-2}, a beat in the SdH oscillations is seen in ρ_{xx} [Fig. 3(b)], indicating the population of the second subband. The occupation of the second subband results in a new scattering channel, giving rise to intersubband scattering.[49] This causes an intermodulation of the two subbands producing the beat.[50–52] The Fourier transform of the data versus inverse magnetic field yields two peaks, one at a frequency $f_1 = 36.4$ T corresponding to a density in the lowest subband $n_{e_1} = 2ef_1/h = 1.76 \times 10^{16}$ m^{-2} (h is Planck's constant) and one peak at the difference frequency $f_1 - f_2 = 33.6$ T. This implies a density in the second subband of $n_{e_2} = 2ef_2/h = 0.14 \times 10^{16}$ m^{-2}. The Fermi level at the onset of the population of the second subband ($E_F = \pi\hbar^2 n_H/m^* = 72$ meV) is very close to the distance between the bottom of the two subbands measured by photoluminescence: $E_2 - E_1 = 75$ meV.[53] This is evidence that the observed beat in the SdH oscillations is not the result of inhomogeneities in the sample. Our ρ_{xx} data do not show any sign of a superposition of SdH oscillations with two frequencies as quite often observed in systems with two occupied subbands.[17,50,52,54] The beat we see in the SdH oscillations is only observed over a very narrow range of densities [$n_H = (1.75 \pm 0.01) \times 10^{14}$ m^{-2}]. As the density is increased further by illumination, any obvious signs of the second subband disappear and the SdH oscillations are observed on a rising background, which becomes stronger with increasing density [Figs. 3(c) and 3(d)]. At the same time, in the Hall effect, ρ_{xy} is seen to deviate from the classical straight line. As will be discussed below, this is evidence for a second type of carrier with a much lower mobility.

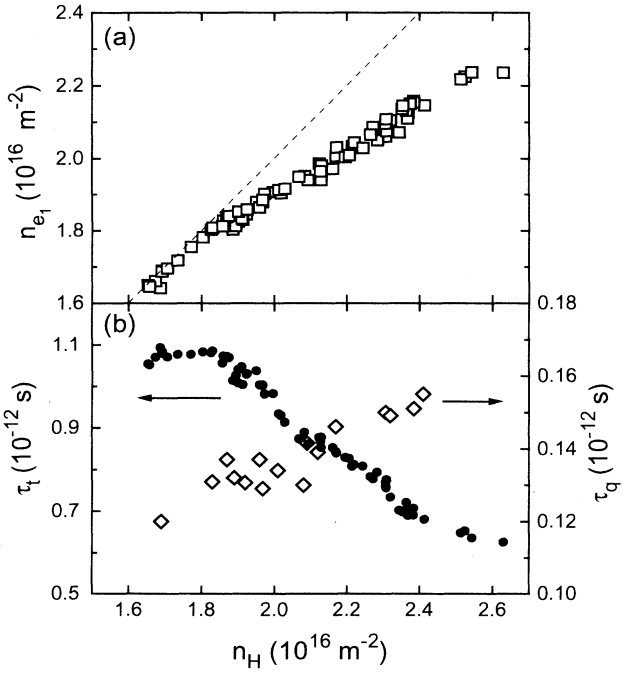

FIG. 4. (a) Electron density n_{e_1} in the lowest subband in the GaAs/$Ga_{0.8}In_{0.2}As$/$Ga_{0.75}Al_{0.25}As$ QW (□) versus the Hall density n_H. The dashed line represents the $n_{e_1} = n_H$ line. (b) The transport lifetime τ_t (•) and the quantum life-time τ_q in the first subband in the $Ga_{0.8}In_{0.2}As$ QW (◇) versus the Hall density n_H.

The density n_{e_1} of the lowest subband in the $Ga_{0.8}In_{0.2}As$ quantum well, obtained from the period of the SdH oscillations, is shown versus the Hall density n_H [see Eq. (2)] in Fig. 4(a). Below $n_H = 1.8 \times 10^{16}$ m^{-2} the small difference between the data points and the dashed $n_{e_1} = n_H$ line is the result of experimental error rather than a consequence of the very small number of carriers in the second subband around $n_H \approx 1.75 \times 10^{16}$ m^{-2}. For densities $n_H \geq 1.85 \times 10^{16}$ m^{-2} however, a large difference between the data points and the line is apparent. This shows that carriers in the $Ga_{0.8}In_{0.2}As$ QW no longer account for the total density beyond $n_H = 1.85 \times 10^{16}$ m^{-2}. At the same value for n_H the transport lifetime $\tau_t = \mu_H m^*/e$, shown in Fig. 4(b), starts to decrease with increasing Hall density.

C. Multisubband occupation and parallel conduction

The resistivity of a multisubband 2DEG or a 2DEG with a parallel conduction layer in the presence of a magnetic field B is usually described by the sheet resistivity tensor $\tilde{\rho}_i$, where the subscript i labels the conducting layer. If the conduction in layer i with electron density n_i is due to a process characterized by a single relaxation time $\tau_{t,i}$ then the Lorentz force leads to[55]

$$\tilde{\rho}_i = \begin{pmatrix} \rho_{0,i} & B/n_i e \\ -B/n_i e & \rho_{0,i} \end{pmatrix} = \begin{pmatrix} \rho_{xx,i} & \rho_{xy,i} \\ -\rho_{xy,i} & \rho_{xx,i} \end{pmatrix}, \quad (4)$$

where $\rho_{0,i} = m_i^*/n_i e^2 \tau_{t,i}$ and m_i^* is the effective mass of the carriers in layer i. The total current in the case of a parallel connected multilayer system is the sum of the currents in the different layers. Thus the total sheet conductivity is the sum of the sheet conductivities of the separate layers.[56] If the conductivity of layer i is given by

$$\tilde{\sigma}_i = \frac{n_i e^2 \tau_{t,i}}{m_i^*} \frac{1}{1+\omega_c^2 \tau_{t,i}^2} \begin{pmatrix} 1 & -\omega_c \tau_{t,i} \\ \omega_c \tau_{t,i} & 1 \end{pmatrix} \quad (5)$$

$$= \begin{pmatrix} D_i & -A_i \\ A_i & D_i \end{pmatrix}, \quad (6)$$

with $\omega_{c,i} = eB/m_i^*$, then the total conductivity of a system with two layers, labeled a and b, is

$$\tilde{\sigma}_{\rm tot} = \tilde{\sigma}_a + \tilde{\sigma}_b = \begin{pmatrix} (D_a + D_b) & -(A_a + A_b) \\ (A_a + A_b) & (D_a + D_b) \end{pmatrix}. \quad (7)$$

After inverting the above equations we obtain for the resistivity

$$\rho_{xx} = \frac{D_a + D_b}{(D_a + D_b)^2 + (A_a + A_b)^2} \quad (8)$$

and

$$\rho_{xy} = -\frac{A_a + A_b}{(D_a + D_b)^2 + (A_a + A_b)^2}. \quad (9)$$

These equations can be simply written in terms of the densities n_a, n_b and the mobilities μ_a, μ_b of the two layers.[56] The expressions are simplified in the case of low magnetic fields (such that $\mu_a B, \mu_b B \ll 1$) so that

$$\rho_{xx} = \frac{1}{e}\frac{1}{n_a\mu_a + n_b\mu_b} = \frac{1}{e}\frac{1}{n_H\mu_H} \quad (10)$$

and

$$\rho_{xy} = \frac{B}{e}\frac{n_a\mu_a^2 + n_b\mu_b^2}{(n_a\mu_a + n_b\mu_b)^2} = \frac{B}{e}\frac{1}{n_H}. \quad (11)$$

Equations (10) and (11) relate the Hall density n_H and the Hall mobility μ_H to the densities n_a and n_b and the mobilities μ_a and μ_b.

We have fitted Eqs. (8) and (9) to the low-field measurements of ρ_{xx} and ρ_{xy} in order to obtain values for the electron density and mobility in the Si δ layer ($n_{e_3} = n_b$ and $\mu_3 = \mu_b$) and the mobility $\mu_1 = \mu_a$ in the first subband in the GaAs/$Ga_{0.8}In_{0.2}As$/$Ga_{0.75}Al_{0.25}As$ QW. Since the number of carriers in the second subband n_{e_2} is small and the transport mobility μ_2 of these carriers is usually a few times smaller than the mobility of the electrons in the first subband,[54] we ignored the second subband in our fit (in the resistivity calculations in Sec. V the second subband is included, but it is found that it has a negligibly small effect on the resistivity values). We used the density in the first subband $n_{e_1} = n_a$, determined from the frequency of the SdH oscillations, as an input parameter. A typical fit is shown in Fig. 5. The agreement between the classical picture and the background of both ρ_{xx} and ρ_{xy} is very good. The resulting parameters are shown in Table I. The values obtained for the density n_{e_3} and the mobility μ_3 indicate that the Si δ layer has a very high electron density and has a mobility that is ~50 times smaller than the mobility in the first subband. Both the high density and the low mobility are typical for parallel conduction in an impurity layer such as the Si δ layer in our case. From the values in Table I, it is easily verified that the mobilities and densities obey the relation $n_H\mu_H = n_{e_1}\mu_1 + n_{e_3}\mu_3$, as implied by Eq. (10).

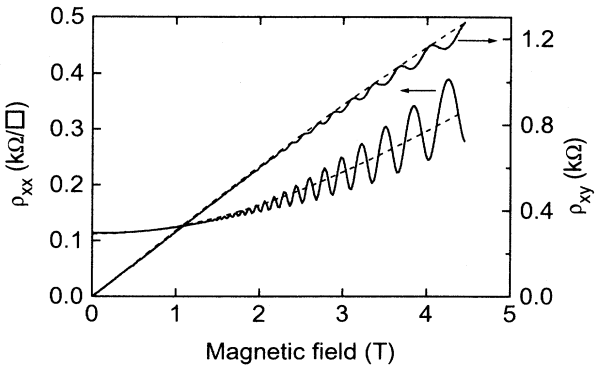

FIG. 5. Fit of the two-carrier model to the low-field ρ_{xx} and ρ_{xy} data at 4.2 K. The Hall density is $n_H = 2.07 \times 10^{16}$ m^{-2}. The dashed line represents the fit with parameters $n_{e_1} = 1.95 \times 10^{16}$ m^{-2}, $\mu_1 = 2.8$ m^2/V s, $n_{e_3} = 1.5 \times 10^{16}$ m^{-2}, and $\mu_3 = 0.06$ m^2/V s.

D. Scattering times

From the temperature dependence of the amplitude of the SdH oscillations (see Sec. IV A) we determined the effective mass to be $m^* = (0.058 \pm 0.005)m_0$ at the dark value of the density (m_0 is the rest mass of the free electron). This is lower than the experimental values for the effective mass for GaAs/$Ga_{1-x}In_xAs$/$Ga_{1-y}Al_yAs$ systems found in the literature, which show a wide spread: from $m^* = 0.063m_0$ (Ref. 57) to $m^* = 0.072m_0$ (Ref. 58) for GaAs/ $Ga_{0.87}In_{0.13}As$/$Ga_{0.7}Al_{0.3}As$ and from $m^* = 0.067m_0$ (Ref. 58) to $m^* = 0.071m_0$ (Ref. 59) for GaAs/$Ga_{0.82}In_{0.18}As$/$Ga_{0.7}Al_{0.3}As$. The difference

TABLE I. Densities and mobilities obtained from the low-field transport data (n_H, μ_H, and n_{e_1}) and from the fit to the two-band model (μ_1, n_{e_3}, and μ_3).

n_H (10^{16} m^{-2})	μ_H (m^2/V s)	$n_{\rm SdH} = n_{e_1}$ (10^{16} m^{-2})	μ_1 (m^2/V s)	n_{e_3} (10^{16} m^{-2})	μ_3 (m^2/V s)
1.67	3.24	1.66	3.31		
1.87	3.25	1.84	3.32	0.7	0.02
1.97	3.02	1.88	3.22	0.8	0.08
2.07	2.65	1.95	2.81	1.5	0.06
2.21	2.50	2.01	2.74	2.4	0.06
2.53	1.98	2.22	2.17	3.9	0.07

might in part be due to the higher In content in our structures.

When m^* is known, the single-particle scattering time can be determined from the decay of the SdH oscillations with decreasing magnetic field by making a so-called Dingle plot of $\ln(\Delta\rho \sinh X/2\rho_0 X)$ versus inverse magnetic field, with $\Delta\rho$ the measured amplitude of the oscillations. The slope of the resulting plot is then inversely proportional to the single-particle scattering time τ_q.[60]

The results of the Dingle analysis are shown in Fig. 4(b). We see that with increasing carrier density the single-particle scattering time increases. By contrast, the transport scattering time, also shown in Fig. 4(b), decreases with increasing carrier density.[61] This apparent contradictory behavior can be understood as follows. The single-particle scattering rate counts every scattering event. However, the transport scattering time in high-density GaAs/$Ga_{1-x}In_xAs$/$Ga_{1-y}Al_yAs$ structures is mainly determined by large-angle scattering events such as cluster scattering due to the nonuniform distribution of In in the $Ga_{1-x}In_xAs$ (Ref. 8) and intersubband scattering).[49] The latter becomes more important when the density increases so that the Fermi level lies in or very close to the second subband. Also cluster scattering increases with increasing density.[8] In contrast, small-angle scattering such as remote ionized impurity scattering due to the ionized Si donors in the δ layer is more effectively screened when the carrier density is large, and the remote ionized impurity scattering is also screened by additional carriers in the second subband and the δ layer. The effect of a reduction in the small-angle scattering, which dominates the single-particle scattering time, outweighs the concurrent increase in the large-angle scattering rate. Consequently, the single-particle scattering time in the first subband increases with density while the transport lifetime decreases.

We do not see any clear effect of the depopulation of the second subband on the Hall mobility or the quantum lifetime in the first subband as has been observed in GaAs/$Ga_{1-x}Al_xAs$ heterojunctions with two occupied subbands.[45] This is likely to be due to the relatively low mobilities in the GaAs/$Ga_{0.8}In_{0.2}As$/$Ga_{0.75}Al_{0.25}As$ heterojunction compared to those in GaAs/$Ga_{1-x}Al_xAs$ structures.

V. LARGE MAGNETIC FIELDS

A. Introduction

At sufficiently high magnetic fields, ρ_{xx} can become vanishingly small and ρ_{xy} shows plateaus in finite ranges of the magnetic field when E_F lies between two separated Landau levels. This feature of electrical transport in high magnetic fields in 2D systems is called the quantized Hall effect[62–65] and has been observed in a wide range of semiconductor heterostructures.

Typical high-field transport data are shown in Fig. 6 for a Hall density of $n_H = 1.9\times10^{16}$ m^{-2}: above 37 T ρ_{xx} becomes very small for the lower temperature T=1.4 K and there is a corresponding quantized plateau in ρ_{xy} at

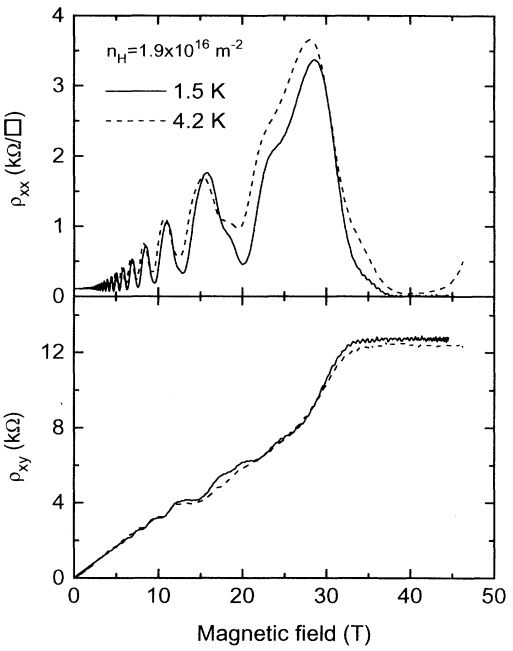

FIG. 6. High-field data for ρ_{xx} and ρ_{xy} at 1.4 K (full line) and at 4.2 K (dashed line) at a Hall density of $n_H = 1.9 \times 10^{16}$ m^{-2}.

12.5 kΩ. The rising background in ρ_{xx} at fields below 30 T is due to parallel conduction in the Si δ layer, which freezes out at 1.4 K and fields $B > 30$ T. For the higher temperature $T = 4.2$ K, there is still some parallel conduction and the high-field minimum in ρ_{xx} is at about 200 Ω/□.

B. Theory

At high magnetic fields the conductivities of a 2D system are given by[38]

$$\sigma_{xx} = \frac{e^2}{\pi^2\hbar}\sum_{N,s}\int dE\left(-\frac{\partial f(E)}{\partial E}\right) \times\left[\frac{\Gamma_N^{xx}}{\Gamma_{N,s}}\right]^2[\pi^2 l^2\Gamma_{N,s}D_{\Gamma_{N,s}}(E)]^2 \tag{12a}$$

and

$$\sigma_{xy} = -\frac{e}{B}\sum_{N,s}\int dE f(E)D_{\Gamma_{N,s}}(E). \tag{12b}$$

Here $f(E)$ is the Fermi-Dirac distribution function, $D_{\Gamma_{N,s}}(E)$ is the density of states for electrons in Landau level N with spin s, $\Gamma_{N,s}$ is the width of the Landau level, and $\Gamma_N^{xx}/\Gamma_{N,s}$ is a dimensionless factor that depends on the type of scattering. The chemical potential μ is determined through the condition of conservation of total concentration of electrons

$$n_e = \sum_{N,s} \int dE f(E) D_{\Gamma_{N,s}}(E). \tag{13}$$

The sum in the above equations runs over the single-particle states whose energies are given by

$$E_{N,s} = (N + \tfrac{1}{2})\hbar\omega_c + s\tfrac{1}{2}g^*\mu_B B, \tag{14}$$

where $s = \pm 1$, g^* is the effective spin-splitting factor, and μ_B is the Bohr magneton. The spin-splitting factor for bulk GaAs is 0.44,[66] but it has been reported that in a high magnetic field g^* starts to oscillate due to exchange enhancement, reaching values as high as 2.5.[48,67] For all the calculations we have used a constant value for g^*=2.0 for the whole range of magnetic fields. This value is larger than the g factor at zero field, but it is near the measured values for this magnetic field range.[48]

The ratio $\Gamma_N^{xx}/\Gamma_{N,s}$ depends on the type of scattering. For short-range scattering Ando *et al.*[38] found

$$\left[\frac{\Gamma_N^{xx}}{\Gamma_{N,s}}\right]^2 = (N + \tfrac{1}{2}). \tag{15}$$

Ando and Uemura[68] calculated this ratio numerically for the case of a semielliptic DOS. They found that for long-range scattering the ratio $(\Gamma_N^{xx}/\Gamma_{N,s})^2$ is smaller than $(N + 1/2)$ and the difference from the short-range scattering result increases with the Landau level index N.

In order to compare our high-magnetic-field data with theory, a Gaussian form for the total DOS has been used

$$D_{\Gamma_{N,s}}(E) = \frac{1}{2\pi l^2} \frac{1}{\sqrt{2\pi}\Gamma_{N,s}} e^{-(E-E_{N,s})^2/2\Gamma_{N,s}^2}, \tag{16}$$

where $l = \sqrt{\hbar/eB}$ is the magnetic length and $1/2\pi l^2$ is the available number of states in each Landau level. In the limit of short-range scatterers Ando *et al.*[38] found for the level broadening $\Gamma_{N,s}$

$$\Gamma_{N,s}^2 = \frac{2}{\pi} e^2 \frac{\hbar^2}{m^{*2}} \frac{B}{\mu_q}, \tag{17}$$

where $\mu_q = e\tau_q/m^*$ is the quantum mobility.

In the center of the Landau levels the electron states are extended while those in the tail are localized and consequently do not contribute to the dissipative part of the conduction. In the phenomenological model of Englert[69] the tails of the DOS that do not contribute to conduction are taken into account by using a Gaussian DOS $D_{\lambda_{N,s}}(E)$ of *extended states* with a width $\lambda_{N,s} < \Gamma_{N,s}$ (see Fig. 7). Substituting this DOS in Eqs. (12b) and (12a) results in

$$\sigma_{xy}\frac{h}{e^2} = -\sqrt{\frac{2}{\pi}} \sum_{N,s} \int dE f(E) \frac{1}{\lambda_{N,s}} e^{-(E-E_{N,s})^2/2\lambda_{N,s}^2} \tag{18a}$$

and

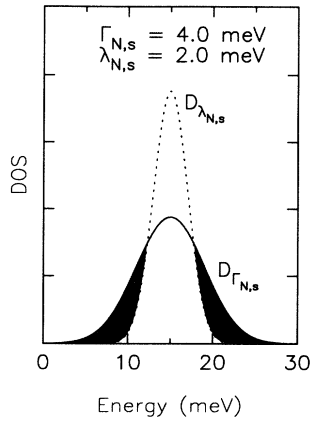

FIG. 7. Gaussian *total* density of states $D_{\Gamma_{N,s}}(E)$ with width $\Gamma_{N,s}$ and the density of *extended* states $D_{\lambda_{N,s}}(E)$ with width $\lambda_{N,s} < \Gamma_{N,s}$ used to calculate the resitivities in the quantized Hall regime.

$$\sigma_{xx}\frac{h}{e^2} = \frac{1}{4}\sum_{N,s} \Gamma_{N,xx}^2 \left(N + \frac{1}{2}\right) \times \int dE \left(-\frac{\partial f(E)}{\partial E}\right) e^{-(E-E_{N,s})^2/\lambda_{N,s}^2}. \tag{18b}$$

In this last equation we introduced the factor $\Gamma_{N,xx}^2 = (\Gamma_N^{xx}/\Gamma_{N,s})^2/(N + 1/2)$, which equals 1 in the case of short-range scatterers. In the evaluation of the Fermi level all the electrons contribute and consequently the total DOS $D_{\Gamma_{N,s}}(E)$ is used.

The approximation of short-range scatterers is clearly not satisfied in the modulation doped heterostructures of the present study. From Ando *et al.*[38] it is obvious that for long-range scattering the peak transverse conductivity decreases rapidly with increasing scattering range. Therefore, in our calculations we used the ratio $\Gamma_{N,xx}$ as a fitting parameter in order to give information about the range of the scattering centers relevant for the present samples.

With changing magnetic field the population of the different Landau levels within one 2D layer changes and it is possible that the electrons tunnel from the QW to the δ layer and vice versa. This results in a Fermi energy that depends on the magnetic field. At $T = 0$ Eq. (13) becomes

$$n_e = \sum_i n_{e_i} = \sum_i \sum_{N,s} \int_0^{E_F} dE D_{\Gamma_{N,s}}^i(E), \tag{19}$$

where the index i indicates the conducting layer. For low temperatures ($T < 10$ K) we expect the Fermi energy to be very close to the $T = 0$ value. For the $B = 0$ case and for low temperatures we can calculate the Fermi energy for a perfect 2DEG from the number of electrons using the relation[38]

$$n_e = \frac{m^*}{\pi\hbar^2}(E - E_F) \ , \tag{20}$$

where E is the bottom of the subband.

When the magnetic field becomes sufficiently large it will affect the equilibrium population of the free electrons in the δ layer. A magnetic field shrinks the electron wave function, leading to an increase of the binding energy of the donor impurities and eventually into the freeze-out of the electrons in the impurity bound states.[70,71] For a structure with a single type of carrier, the onset of the freeze-out regime corresponds to the magnetic field at which ρ_{xy} starts to increase abruptly with increasing B. In our calculations we have obtained the threshold field $B_{\rm thr}$ from the experimental ρ_{xy} data. For magnetic fields beyond this threshold field we can approximate the number of electrons by[72,73]

$$n_e = n_0 e^{-\epsilon_B/k_B T} \ , \tag{21}$$

where n_0 is the density below the freeze-out threshold and ϵ_B is the electron binding energy which depends on the magnetic field through

$$\epsilon_B = b(B - B_{\rm thr})^{1/3}, \tag{22}$$

where b is a constant that is taken as a fitting parameter. This reduction of the number of electrons results in a decrease of the Fermi energy and consequently leads to a lowering of the Landau level occupation and an increase in ρ_{xy}.

C. Comparison with experiment

1. The QHE in the $Ga_{0.8}In_{0.2}As$ QW

In Fig. 8 we show the measured resistivities (full curves) ρ_{xx} and ρ_{xy} of the unilluminated structure with an electron concentration of $n_H = 1.69 \times 10^{16}$ m^{-2} at T=1.4 and 4.2 K. At this density only the lowest subband in the GaAs/$Ga_{0.8}In_{0.2}As$/$Ga_{0.75}Al_{0.25}As$ quantum well is occupied and n_H equals the total electron density in the structure. There is no parallel conduction in the δ layer and the system shows the QHE. At 1.4 K the ρ_{xy} plateau at a Landau level filling factor $\nu = 2$ extends over a field range of 10 T and corresponds to a $\rho_{xx} = 0$ minimum of the same width. Deep minima in ρ_{xx} are also seen at filling factors $\nu = 4$ and $\nu = 6$.

TABLE II. Parameters for the two lowest electron concentrations [$n_H = 1.69 \times 10^{16}$ m^{-2} (Fig. 8) and $n_H = 1.84 \times 10^{16}$ m^{-2} (Fig. 9)] when only the lowest subband in the $Ga_{0.8}In_{0.2}As$ QW (index 1) is occupied.

	Fig. 8 Index 1	Fig. 9 Index 1
Fitting parameters		
Γ_i (meV)	$0.8\sqrt{B}$	$0.8\sqrt{B}$
λ_i (meV)	$0.2\sqrt{B}$	$0.24\sqrt{B}$
$\Gamma_{N,xx}$	0.65	0.8
Physical parameters		
Γ_δ (meV)	$2.46\sqrt{B}$	$2.46\sqrt{B}$
μ_i (m^2/V s)	3.31	3.32
μ_{q_i} (m^2/V s)	0.31	0.31
n_{e_i} ($\times 10^{16}$ m^{-2})	1.63	1.8

Figure 8 also shows the theoretical calculations for high fields using the Englert model described above (dotted curves). The parameters used for the calculations are shown in Table II. The agreement between the theoretical calculations and the experimental data for ρ_{xx} and ρ_{xy} is fairly good. Notice (see Table II) that we took $\Gamma_{N,xx} = 0.65 < 1$, which indicates that there is a significant contribution from small-angle scattering. This is in agreement with Fig. 4, which shows that the transport relaxation time is almost an order of magnitude larger than the quantum lifetime, a characteristic feature of small-angle scattering. This also agrees with the fact that the

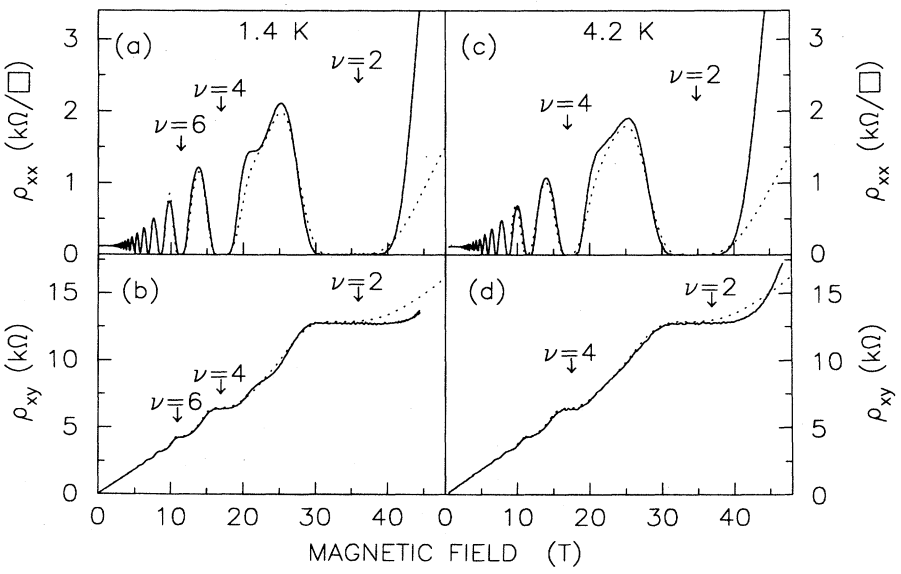

FIG. 8. ρ_{xx} and ρ_{xy} at (a) and (b) 1.4 K and (c) and (d) 42.K at a Hall density of $n_H = 1.69 \times 10^{16}$ m^{-2}. The full lines represent the experimental data and the dotted line shows the theoretical results.

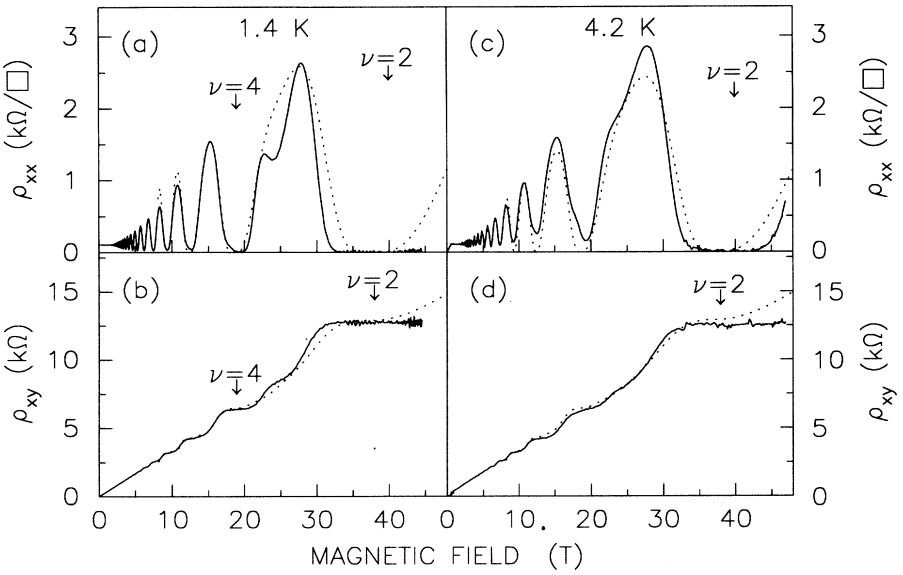

FIG. 9. ρ_{xx} and ρ_{xy} at (a) and (b) 1.4 K and at (c) and (d) 4.2 K at a Hall density of $n_H = 1.84 \times 10^{16}$ m^{-2}. The full lines represent the experimental data and the dotted line shows the theoretical calculations. No magnetic freeze-out is included in these calculations.

width of the Landau levels Γ_i is much smaller than the width Γ_δ we would infer from a theory with δ-function scatterers [$\Gamma_i/\Gamma_\delta = 0.3$; see Eq. (17)]. For T=1.4 K the agreement between theory and experiment is rather good for both ρ_{xx} and ρ_{xy}. For $B > 40$ T the agreement is less satisfactory, indicating a smaller value for the width of the lowest Landau level. Note that in our analysis we assumed Γ_i, λ_i, and $\Gamma_{N,xx}$ to be independent of the Landau level index N in order to limit the number of fitting parameters. It is known that for non-δ-function scatterers this assumption breaks down.[38]

A similar discrepancy between theory and experiment at fields > 40 T is seen for $T = 4.2$ K. The observed spin splitting in ρ_{xx} at $B \approx 22$ T hardly shows up in the theoretical results, indicating an exchange enhanced spin-splitting factor[48,67] at this field that is larger than the value $g^* = 2.0$ we used in the calculations.

2. *Parallel conduction*

In Fig. 9 ρ_{xx} and ρ_{xy} are shown for a Hall density $n_H = 1.84 \times 10^{16}$ m^{-2} at $T = 1.4$ and 4.2 K. The parameters used in the calculations are given in Table II. From Fig. 9 we notice that there is reasonable agreement between theory and experiment for 1.4 K when we assume that the ground subband in the δ layer is not populated. However, at 4.2 K the experimental data clearly show that (i) the minima in ρ_{xx} below 30 T are no longer zero and (ii) ρ_{xy} slightly deviates to lower values than expected from an extrapolation from the $B = 0$ behavior. Both experimental findings indicate that there is parallel conduction in the δ layer or in the second subband of the QW. This is in agreement with the results of Sec. IV C and Table I, where we found that for $n_H = 1.87 \times 10^{16}$ m^{-2} the ground subband in the δ layer is populated with a density $n_{e_3} \approx 0.7 \times 10^{16}$ m^{-2}. For $T = 1.4$ K however, the magnetic freeze-out of these carriers occurs already at small magnetic fields. Therefore those carriers are not included in the calculation. From Eq. (21) it is obvious that at 4.2 K the effect of the magnetic freeze-out is strongly weakened, resulting in parallel conduction and ρ_{xx} minima that are no longer zero. But for $B > 30$ T the electrons in the Si δ layer are again practically frozen out so that the ρ_{xx} minima become almost zero and ρ_{xy} exhibits a plateau at the quantized value of $h/2e^2$.

In Figs. 10(a) and 10(b) we show the resistivities ρ_{xx} and ρ_{xy} at 1.4 K for $n_H = 1.97 \times 10^{16}$ m^{-2}. The parameters used to obtain the theoretical curves (dash-dotted lines) are given in Table III. The experimental ρ_{xy} data (solid line) in Fig. 10(b) show a steep increase at $B = 36$ T from 6.4 kΩ to 12.8 kΩ, which coincides with a steep drop in ρ_{xx}. These changes in the transport

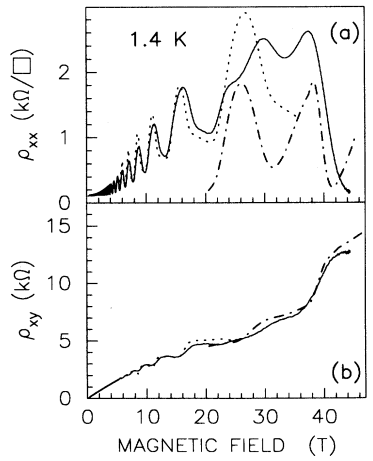

FIG. 10. (a) ρ_{xx} and (b) ρ_{xy} at 1.4 K at a Hall density of $n_H = 1.95 \times 10^{16}$ m^{-2}; comparison between experiment (full line) and theory (dashed line, the low field region where the Isihara-Smrčka model is used for both the 2DEG's; dotted line, the regime where the 2DEG in the QW is described by the Englert model and the 2DEG in the δ layer is described by the Isihara-Smrčka model; dot-dashed line, the regime where both 2DEG's are described by the Englert model).

data can again be attributed to the magnetic freeze-out of the electrons in the δ layer. In the calculation we used $b = 0.1$ meV/T$^{1/3}$. We used as threshold field $B_{\rm thr} = 36$ T. The binding energy is of the order of 0.1 meV at $B = 37$ T, at which point it equals the thermal energy k_BT for $T = 1.4$ K. The electron single-particle relaxation times differ by almost two orders of magnitude for the ground subband of the QW as compared to the ground subband of the δ layer. Therefore the field where the Isihara-Smrčka model breaks down is much higher for the δ layer than for the QW. To take this into account in our calculations we divided the high-magnetic-field range ($B > 5$ T) into two different regimes: for magnetic fields $B < 27$ T the Englert model is used for the ground subband of the QW where $\omega_c\tau_q > 1$, while the Isihara-Smrčka model is applied to the ground subband of the δ layer. At fields $B > 27$ T we applied the Englert model for both layers. The agreement between theory and experiment for both ρ_{xx} and ρ_{xy} is fairly good for fields lower than 25 T and for fields larger than 35 T. There are discrepancies in the area between 25 and 35 T, which are probably due to the simple approach that we used for the magnetic freeze-out model and the transition between different theoretical models. We have also not taken into account changes in the shape of the potential well and in the transport and quantum mobilities, which are a consequence of the fast descent of the number of the electrons in the δ layer due to the magnetic freeze-out.

3. *The QHE in two layers*

Figures 11(a) and 11(b) show ρ_{xx} and ρ_{xy} at 1.4 K for a Hall density of $n_H = 2.05\times10^{16}$ m^{-2}. The corresponding Fermi level E_F and the carrier densities n_{e_i} in the different subbands i are given in Figs. 11(c) and 11(d). In this calculation we used $m^* = 0.067m_0$ and $0.058m_0$ for the electron effective masses in GaAs and $Ga_{0.8}In_{0.2}As$, respectively. The $B = 0$ values of the Fermi energy for each subband are calculated from Eq. (20). The parameters we used in the calculations and the Landau-level broadening in case of δ scattering [Eq. (17)] are shown in Table IV. In our calculations we have extended the two-carrier model discussed in Sec. IV C to the case of three conducting layers and we have used a constant $\Gamma_{N,xx} = 0.75$ for the QW for all the Landau levels. For the δ layer we have used $\Gamma_{N,xx} = 0.95$ for all Landau levels. This reflects the fact that in the δ layer the scattering is predominantly due to the large concentration of background impurities (Si donors) resulting in large-angle scattering very similar to δ-function scattering.

TABLE III. Fitting parameters for the theoretical calculations in Fig. 10 ($n_H = 1.95 \times 10^{16}$ m^{-2}). The indices 1 and 3 refer to the first subband in the $Ga_{0.8}In_{0.2}As$ QW and the lowest subband in the Si δ layer, respectively.

	Index 1	Index 3
Fitting parameters		
Γ_i (meV)	$1.2\sqrt{B}$	$3.50\sqrt{B}$
λ_i (meV)	$0.8\sqrt{B}$	$2.3\sqrt{B}$
$\Gamma_{N,xx}$	0.75	0.9
Physical parameters		
Γ_δ (meV)	$2.27\sqrt{B}$	$7.3\sqrt{B}$
μ_i (m^2/Vs)	2.82	0.05
μ_{q_i} (m^2/Vs)	0.38	0.048
n_{e_i} ($\times10^{16}$ m^{-2})	1.89	0.9

At $B = 0$ there are two subbands occupied in the QW and one in the δ layer. As can be seen from Fig. 11(b), the second subband in the $Ga_{0.8}In_{0.2}As$ QW has a very low carrier concentration compared to the other two layers; therefore it contributes very little to the conductivities. We used the following parameters for the second subband in our calculations: $n_{e_2} = 0.05 \times 10^{16}$ m^{-2}, $\Gamma_2 = 1.60\sqrt{B}$ meV, $\lambda_2 = 1.25\sqrt{B}$ meV, $\mu_2 = 0.3$ m^2/V s, and $\mu_{q_2} = 0.1$ m^2/V s. These values are only accurate to within a factor of 3. This low accuracy in the determina-

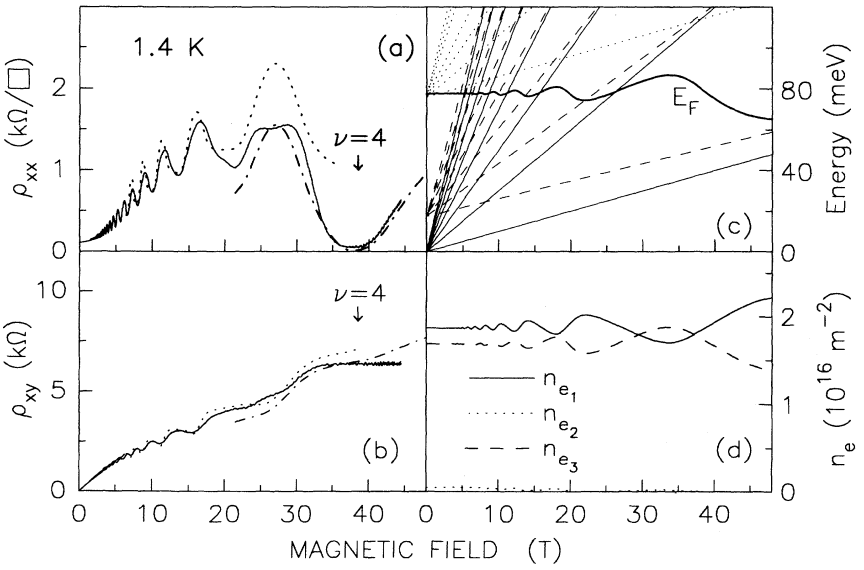

FIG. 11. (a) ρ_{xx} and (b) ρ_{xy} at 1.4 K at a Hall density of $n_H = 2.05 \times 10^{16}$ m^{-2}; comparison between experiment (full line) and theory (dashed line, the low field region where the Isihara-Smrčka model is used for both the 2DEG's; dotted line, the regime where the 2DEG in the QW is described by the Englert model and the 2DEG in the δ layer is described by the Isihara-Smrčka model; dot-dashed line, the regime where both 2DEG's are described by the Englert model). (c) shows the Landau levels and the Fermi energy E_F and (d) shows the electron densities in the different layers (full line and dotted line, first and second subband in the QW, respectively, dashed line, the 2DEG in the δ layer.

TABLE IV. Fitting and physical parameters for the theoretical calculations in Fig. 11 ($n_H = 2.05 \times 10^{16}$ m^{-2}). The indices 1 and 3 refer to the first subband in the $Ga_{0.8}In_{0.2}As$ QW and the lowest subband in the Si δ layer, respectively.

	Index 1	Index 3
Fitting parameters		
Γ_i (meV)	$1.4\sqrt{B}$	$3.5\sqrt{B}$
λ_i (meV)	$0.95\sqrt{B}$	$2.25\sqrt{B}$
$\Gamma_{N,xx}$	0. 75	0.95
Physical parameters		
Γ_δ (meV)	$2.2\sqrt{B}$	$7.90\sqrt{B}$
μ_i (m^2/V s)	3.00	0.05
μ_{q_i} (m^2/V s)	0.4	0.04
n_{e_i} ($\times 10^{16}$ m^{-2})	1.85	1.65

tion of these parameters is due to the fact that because of the low electron density n_{e_2} there is practically no contribution of this layer to the resistivities ρ_{xx} and ρ_{xy}.

An oscillatory electron density in the different electron layers is observed. This is due to the pinning of the Fermi energy in the δ layer combined with electron flow between the two layers. At 37 T the lowest subband in the QW and the lowest subband in the δ layer have nearly equal densities. Due to the high electron density in the δ layer magnetic freeze-out no longer occurs in the experimentally accessible magnetic-field range. However, the magnetic field is strong enough to introduce Landau quantization effects in the low-mobility 2DEG in the δ layer. As a result we have two parallel 2DEGs, each showing the QHE at a Landau level filling factor of 2 at $B \approx 37$ T, which results in a total filling factor $\nu = 4$. Consequently, a deep minimum in ρ_{xx} and a quantized Hall plateau at $\rho_{xy} = h/4e^2 = 6.5$ kΩ are observed.

As is apparent from Fig. 11, satisfactory agreement between theory and experiment has been obtained. The agreement is best at low magnetic fields where the Isihara-Smrčka model is used. For $B > 35$ T there is a slight disagreement between theory and experiment in the ρ_{xy} results. This is probably due to the fact that ρ_{xy} is still quantized despite that $\rho_{xx} \neq 0$. This makes it difficult to achieve perfect agreement for both ρ_{xx} and ρ_{xy} within our simple theoretical framework.

VI. CONCLUSION

The magnetoresistance ρ_{xx} and the Hall resistance ρ_{xy} in a $GaAs/Ga_{0.8}In_{0.2}As/Ga_{0.75}Al_{0.25}As$ heterostructure with a Si δ layer parallel to the $Ga_{0.8}In_{0.2}As$ QW were measured in magnetic fields up to 50 T. We provide a coherent description of the transport phenomena using two subbands in the $Ga_{0.8}In_{0.2}As$ QW and one subband in the Si δ layer.

Comparing the low-field data with the semiclassical two-band model, we showed that in the illuminated structure the δ layer has a high concentration of carriers with a low mobility. Changing the electron density through illumination has a strong, but opposite effect on the transport scattering time and the quantum scattering time.

For a theoretical description of ρ_{xx} and ρ_{xy} for the complete experimental magnetic field range, we used the Isihara-Smrčka model to fit the SdH oscillations in the low-field regime where $\omega_c\tau_q < 1$. The *low-field* range extends up to 30 T for the Si δ layer while for the QW this range does not extend beyond 5 T. For the high-field regimes we employed the Englert model, which is basically a phenomenological picture for the quantum Hall effect. For low carrier densities in the δ layer we had to include magnetic freeze-out to account for the loss of carriers at high fields in this layer. We combined these different models using the two-band model to obtain values for ρ_{xx} and ρ_{xy}. Using only the level broadening, the binding energy and the freeze-out threshold field as fitting parameters we obtained satisfactory agreement between the experimental data and theory. For fields $B > 37-40$ T the agreement is less satisfactory, which is probably due to the fact that we assumd a level broadening independent of the Landau level index.

Since the second subband in the $Ga_{0.8}In_{0.2}As$ QW has a very small amount of carriers as compared to the first subband, this contribution to conduction is hard to detect in transport experiments. The remaining discrepancies between theory and experiment can also be partly due to a lack of precise information about the second subband and the subband structure in the Si δ layer.

ACKNOWLEDGMENTS

M.v.d.B and V.C.K. acknowledge the support of the Human Capital and Mobility Programme of the EC. F. M. P. is supported by the Belgian National Fund for Scientific Research. This work was also supported by a cooperation program of the Interuniversity Microelectronics Center and the Flemish Universities.

* On leave from Katholieke Universiteit Leuven, Department of Physics, Celestijnenlaan 200D, B-3001 Leuven, Belgium.

[1] H. L. Störmer, R. Dingle, A. C. Gossard, W. Wiegmann, and M. D. Sturge, Solid State Commun. **29**, 705 (1979).
[2] R. Dingle, H. L. Störmer, A. C. Gossard, and W. Wiegmann, Appl. Phys. Lett. **33**, 665 (1978).
[3] C. T. Foxon, J. J. Harris, D. Hilton, J. Hewett, and C. Roberts, Semicond. Sci. Technol. **4**, 582 (1989).
[4] L. Pfeiffer, K. W. West, H. L. Störmer, and K. W. Baldwin, Appl. Phys. Lett. **55**, 1888 (1989).
[5] K. Lee, M. S. Shur, J. T. Drummond, and H. Morkoç, J. Appl. Phys. **54**, 6432 (1983).
[6] W. Waluckiewicz, H. E. Ruda, J. Lagowski, and H. C. Gatos, Phys. Rev. B **30**, 4571 (1984).
[7] H. Ohno, J. K. Luo, K. Matsuzaki, and H. Hasegawa, Appl. Phys. Lett. **54**, 36 (1988).

[8] J. K. Luo, H. Ohno, K. Matsuzaki, and H. Hasegawa, Jpn. J. Appl. Phys. **27**, 1831 (1988).
[9] J. J. Rosenberg, M. Benlamri, P. D. Kirchner, J. M. Woodall, and G. D. Pettit, IEEE Electron Device Lett. **EDL-6**, 491 (1986).
[10] S. Adachi, J. Appl. Phys. **53**, 8775 (1982).
[11] S. Adachi, J. Appl. Phys. **58**, R1 (1985).
[12] S. Tiwari and D. J. Frank, Appl. Phys. Lett. **60**, 630 (1992).
[13] T. G. Andersson, Z. G. Chen, V. D. Kulakovskii, A. Uddin, and J. T. Vallin, Appl. Phys. Lett. **51**, 752 (1987).
[14] I. J. Fritz, P. L. Gourley, and L. R. Dawson, Appl. Phys. Lett. **51**, 1004 (1987).
[15] A. Zrenner, H. Reisinger, F. Koch, and K. Ploog, in *Proceedings of the 17th International Conference on the Physics of Semiconductors, San Francisco, 1984*, edited by J. D. Chadi and W. A. Harrison (Springer, New York, 1985), p. 325.
[16] E. F. Schubert, J. E. Cunningham, W. T. Tsang, and G. L. Timp, Appl. Phys. Lett. **51**, 1170 (1987).
[17] J. E. Cunningham, W. T. Tsang, G. Timp, E. F. Schubert, A. M. Chang, and K. Uwusu-Sekyere, Phys. Rev. B **37**, 4317 (1988).
[18] E. F. Schubert, *Doping in III-V Semiconductors* (Cambridge University Press, Cambridge, 1993), p. 458.
[19] T. Mimura, S. Hiyamizu, T. Fujii, and K. Nambu, Jpn. J. Appl. Phys. **19**, L225 (1980).
[20] T. N. Theis, P. M. Mooney, and S. L. Wright, Phys. Rev. Lett. **60**, 361 (1988).
[21] P. M. Mooney, Semicond. Sci. Technol. **6**, B1 (1991).
[22] E. F. Schubert, *Doping in III-V Semiconductors* (Ref. 18), p. 355.
[23] S. Luryi and A. Kastalsky, Appl. Phys. Lett. **45**, 164 (1984).
[24] H. Tian, K. W. Kim, and M. A. Littlejohn, J. Appl. Phys. **69**, 4123 (1991).
[25] D. G. Liu, T. C. Chin, C. P. Lee, and H. L. Hwang, Solid-State Electron. **34**, 253 (1991).
[26] M. Kudo, T. Mishima, T. Tanimoto, and M. Washima, Jpn. J. Appl. Phys. **33**, 971 (1994).
[27] D. A. Syphers, K. P. Martin, and R. J. Higgins, Appl. Phys. Lett. **49**, 534 (1986).
[28] J. J. Harris, Meas. Sci. Technol. **2**, 1201 (1991).
[29] A. Zrenner, F. Koch, J. Leotin, M. Goiran, and K. Ploog, Semicond. Sci. Technol. **3**, 1132 (1988).
[30] Q.-Y. Ye, A. Zrenner, F. Koch, and K. Ploog, Semicond. Sci. Technol. **4**, 500 (1989).
[31] M. van der Burgt, A. Van Esch, F. M. Peeters, M. Van Hove, G. Borghs, and F. Herlach, Physica B **184**, 211 (1993).
[32] M. van der Burgt, V. C. Karavolas, F. M. Peeters, J. Singleton, R. J. Nicholas, F. Herlach, J. J. Harris, M. Van Hove, and G. Borghs, in *Proceedings of the 11th International Conference on High Magnetic Fields in Semiconductor Physics, Boston, 1994*, edited by D. Heiman (World Scientific, Singapore, in press).
[33] L. Kapitan (private communication).
[34] W. J. Siertsema and H. Jones, IEEE Trans. Magn. **30**, 1809 (1994).
[35] F. Herlach, L. Van Bockstal, M. van der Burgt, and G. Heremans, Physica B **155**, 61 (1989).
[36] M. van der Burgt, P. Thoen, F. Herlach, F. M. Peeters, J. J. Harris, and C. T. Foxon, Physica B **177**, 409 (1992).
[37] J. R. Mallett, P. M. W. Oswald, R. G. Clark, M. van der Burgt, F. Herlach, J. J. Harris, and C. T. Foxon, in *High Magnetic Fields in Semiconductor Physics III*, edited by G. Landwehr (Springer, Berlin, 1992), p. 277.
[38] T. Ando, A. B. Fowler, and F. Stern, Rev. Mod. Phys. **54**, 437 (1982).
[39] F. Stern and S. Das Sarma, Phys. Rev. B **30**, 840 (1984); G. A. M. Hurkx and W. van Haeringen, J. Phys. C **18**, 5617 (1985); S. Trott, G. Paasch, G. Gobsch, and M. Trott, Phys. Rev. B **39**, 10 232 (1989).
[40] A. Isihara and L. Smrčka, J. Phys. C **19**, 6777 (1986).
[41] P. T. Coleridge, R. Stoner, and R. Fletcher, Phys. Rev. B **39**, 1120 (1989).
[42] M. A. Paalanen, D. C. Tsui, and J. C. M. Hwang, Phys. Rev. Lett. **51**, 2226 (1983); F. F. Fang, T. P. Smith III, and S. L. Wright, Surf. Sci. **196**, 310 (1988).
[43] J. P. Harrang, R. J. Higgins, R. K. Goodall, P. R. Jay, M. Laviron, and P. Delescluse, Phys. Rev. B **32**, 8126 (1985).
[44] U. Bockelmann, G. Abstreiter, G. Weimann, and W. Schlapp, Phys. Rev. B **41**, 7864 (1990).
[45] R. M. Kusters, F. A. Wittekamp, J. Singleton, J. A. A. J. Perenboom, G. A. C. Jones, D. A. Ritchie, J. E. F. Frost, and J.-P. André, Phys. Rev. B **46**, 10 207 (1992).
[46] H. Aoki and H. Kamimura, Solid State Commun. **21**, 45 (1977).
[47] R. Joynt and R. E. Prange, Phys. Rev. B **29**, 3303 (1984).
[48] Th. Englert, D. C. Tsui, A. C. Gossard, and Ch. Uihlein, Surf. Sci. **113**, 295 (1982).
[49] H. L. Störmer, A. C. Gossard, and W. Wiegmann, Solid State Commun. **41**, 707 (1982).
[50] P. T. Coleridge, Semicond. Sci. Technol. **5**, 961 (1990).
[51] S. E. Schacham, E. J. Haugland, and S. A. Alterovitz, Phys. Rev. B **45**, 13 417 (1992).
[52] D. R. Leadley, R. Fletcher, R. J. Nicholas, F. Tao, C. T. Foxon, and J. J. Harris, Phys. Rev. B **46**, 12 439 (1992).
[53] C. M. van Es, T. J. Eijkemans, J. H. Wolter, R. Pereira, M. Van Hove, and M. Van Rossum, J. Appl. Phys. **74**, 6242 (1993).
[54] H. van Houten, J. G. Williamson, M. E. I. Broekaart, C. T. Foxon, and J. J. Harris, Phys. Rev. B **37**, 2756 (1988).
[55] N. W. Ashcroft and N. D. Mermin, *Solid State Physics* (Holt Saunders International, Philadelphia, 1976), p. 240.
[56] M. J. Kane, N. Apsley, D. A. Anderson, L. L. Taylor, and T. Kerr, J. Phys. C **18**, 5629 (1985).
[57] J. K. Luo, H. Ohno, K. Matsuzaki, and H. Hasegawa, Jpn. J. Appl. Phys. **27**, 1831 (1988).
[58] L. V. Butov, V. D. Kulakovskii, T. G. Andersson, and Z. G. Chen, Phys. Rev. B **42**, 9472 (1990).
[59] H. Brugger, H. Müssig, C. Wölk, K. Kern, and D. Heitmann, Appl. Phys. Lett. **59**, 2739 (1991).
[60] Strictly speaking, this treatment is valid only in the case that one subband is occupied. However, we can also carry out this Dingle analysis for larger densities such that the second subband and/or the δ layer are occupied and when no intermodulation of the subbands is observed. This is justified under the assumption that the decay of the SdH oscillations from the first subband is only determined by the single-particle scattering time in this subband and is independent of the featureless background in ρ_{xx} due to the other conduction channels.
[61] The average transport scattering time, defined as $\tau_t = \mu_H m^*/e$ and shown in Fig. 4, roughly follows the transport scattering time in the first subband (see Table I).
[62] K. von Klitzing, G. Dorda, and M. Pepper, Phys. Rev. Lett. **45**, 494 (1980).
[63] R. E. Prange, Phys. Rev. B **23**, 4802 (1981).

[64] S. M. Girvin, A. H. McDonald, and P. M. Platzman, Phys. Rev. B **33**, 2481 (1986).
[65] *The Quantum Hall Effect*, edited by R. E. Prange and S. M. Girvin (Springer, New York, 1987).
[66] C. Weisbuch and C. Hermann, Phys. Rev. B **15**, 816 (1977).
[67] R. J. Nicholas, R. J. Haug, K. von Klitzing, and G. Weimann, Phys. Rev. B **37**, 1294 (1988).
[68] T. Ando and Y. Uemura, J. Phys. Soc. Jpn. **36**, 959 (1974).
[69] Th. Englert, in *Application of High Magnetic Fields in Semiconductor Physics II*, edited by G. Landwehr (Springer, Berlin, 1983), p. 165.
[70] Y. Yafet, R. W. Keyes, and E. N. Adams, J. Phys. Chem. Solids **1**, 137 (1956).
[71] J. J. Mareš, X. Feng, F. Koch, A. Kohl, and J. Krištofic, Phys. Rev. B **50**, 5213 (1994).
[72] O. Beckman, E. Hanamura, and L. J. Neuringer, Phys. Rev. Lett. **18**, 773 (1967).
[73] K. A. Amirkhanov, R. I. Bashirov, and A. Y. Mollaev, Fiz. Tverd. Tela (Leningrad) **13**, 849 (1971) [Sov. Phys. Solid State **13**, 701 (1971)].